Research Article | Vol. 26, No. 23 | 12 Nov 2018 | OPTICS EXPRESS 30435
Optics EXPRESS

Optimizing illumination for full field imaging at high brilliance hard X-ray synchrotron sources

O. Márkus,[1] I. Greving,[2] E. Kornemann,[1] M. Storm,[3] F. Beckmann,[2] J. Mohr,[1] and A. Last[1,*]

[1]Institute of Microstructure Technology (IMT), Karlsruhe Institute of Technology (KIT), Hermann-von-Helmholtz-Platz 1, 76344 Eggenstein-Leopoldshafen, Germany
[2]Institute of Materials Research, Helmholtz Zentrum Geesthacht, Max-Plank-Str. 1, 21502 Geesthacht, Germany
[3]Diamond Light Source Ltd, Didcot, Oxfordshire OX11 0DE, United Kingdom
*arndt.last@kit.edu

Abstract: A new technique is presented to overcome beam size limitation in full field imaging at high brilliance synchrotron sources using specially designed refractive X-ray optics. These optics defocus the incoming beam in vertical direction and reshape the intensity distribution from a Gaussian to a more desirable top-hat-shaped profile at the same time. With these optics X-ray full-field imaging of extended objects becomes possible without having to stack several scans or applying a cone beam geometry in order to image the entire specimen. For in situ experiments in general and for diffraction limited sources in particular this gain in field of view and the optimization of the intensity distribution is going to be very beneficial.

1. Introduction

X-ray imaging techniques like tomography are commonly used at lab and at synchrotron sources for example in the fields of material science, medicine or biology [1–7]. Whereas synchrotron sources offer high brilliance, the beam size in particular in vertical direction is often strongly limited. In addition, the intensity profile of such an undulator source is approximately Gaussian shaped in vertical direction with a FWHM in the range of a few millimeters only [8]. This is a strong limitation for many experiments, in particular full field imaging techniques at 3rd generation synchrotron sources [9,10]. Objects larger than the illuminated field cannot be imaged directly: Image stitching [10] or enlarged cone beam projection [11] have to be applied to overcome this limitation often leading to artefacts in the final reconstructed volume. Time consuming acquisition of several height scans and a more complex image reconstruction are the drawbacks for such full field imaging approaches. In biological studies the additional dose load due to necessarily overlapping fields of view generates problems and often filters are used to reduce the flux at the sample. In particular for *in situ* and time resolved experiments a stitching of different height step scans is often not possible. One way of overcoming this limitation is to use enlarged cone beam projection. Here, however, a virtual source has to be formed by additional X-ray optics. The alignment is often very time consuming and the reconstruction cannot be performed using the parallel beam geometry approach. Another drawback of a 3rd generation X-ray beam is the typical Gaussian intensity profile, leading to differences in the signal to noise ratio between the high-illumination center region and those regions illuminated by the low-intensity tails. A top-hat like beam profile would therefore be very beneficial for full field imaging techniques in general.

There are plenty of examples of how to adjust the beam profile for a certain purpose in visible light optics [12], nevertheless so far mainly focusing concepts have been transferred to the hard X ray regime. For focusing X-rays at energies above approximately 10 keV refractive X ray optics are used, as for these energies the absorption of the lens materials decreases [13–17]. Using a refractive line focus lens to get an enlarged beam after the focal plane is not a suitable way to enlarge the vertical beam size, as in this case the

#336039 https://doi.org/10.1364/OE.26.030435
Journal © 2018 Received 28 Jun 2018; revised 25 Sep 2018; accepted 6 Oct 2018; published 6 Nov 2018

Optics EXPRESS

absorption in the lens material would be too high and the intensity distribution in the beam would get even worse.

At the Institute of Microstructure Technology at Karlsruhe Institute of Technology (KIT/IMT) we have developed refractive beam shaping optics to overcome beam dimension limitations for full field imaging at high brilliance synchrotron sources. In the following we describe the concept, the realization and the results of first performance studies using synchrotron micro computed tomography (SRμ-CT).

2. Optical design and function

The intention of these new beam shaping optics is to redistribute the incoming narrow Gaussian beam intensity distribution into a broad rectangular distribution with high homogeneity (see Fig. 1). As a consequence, it is necessary to design optics, which allow redistributing incoming light from areas close to the optical axis (high intensity) into wider areas and concentrating the incoming light from parts of the Gaussian tails into smaller areas (see Fig. 1).

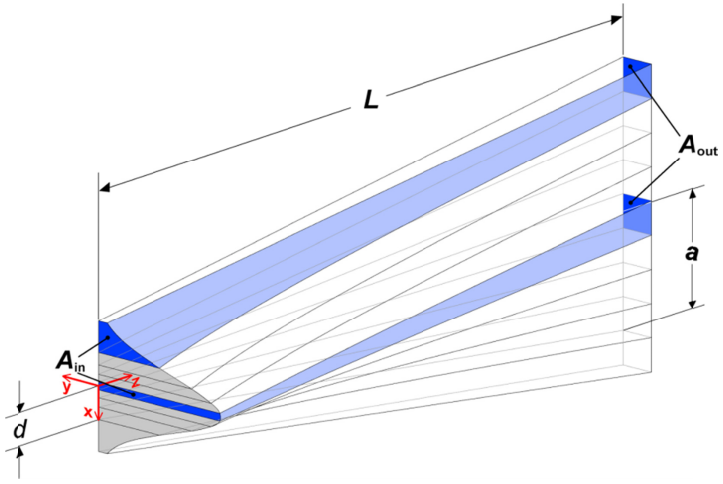

Fig. 1. Incident Gaussian beam intensity (left) transformed into desired top-hat profile (right).

In order to achieve this, the focal length of the lens has to vary across the entrance aperture. Since the beam profile shall be widened, the focal length of the required defocusing lens has to be negative. Close to the optical axis the lens has to have locally a short focal length, whereas far from the optical axis the focal length has to become larger. The optical axis is defined as the z-direction, the x- and y directions are perpendicular to the optical axis (see Fig. 1).

With a Gaussian intensity distribution given in vertical beam direction the intensity I_0 in the center of the beam as a function of the distance from the lens center is given by:

$$I(x) = I_0 e^{-kx^2}. \tag{1}$$

where x is the vertical distance from the center of the beam and k is a constant. Thus the integrated intensity in the area limited to $x = c$ and $x = d$ becomes

$$\int_c^d I(x)dx = \frac{I_0}{2}\sqrt{\frac{\pi}{k}}\left[erf(\sqrt{k}d) - erf(\sqrt{k}c)\right]. \tag{2}$$

The total intensity in a symmetric Gaussian beam profile integrated over a width D is

$$I_{\text{total}} = \int_{-\frac{D}{2}}^{\frac{D}{2}} I(x)dx = I_0\sqrt{\frac{\pi}{k}}erf\left(\sqrt{k}\frac{D}{2}\right). \tag{3}$$

Optics EXPRESS

Assuming the width of the requested top-hat distribution is B. In the case of a loss-free, perfect optics, the total intensity I_{total} will stay constant and the top-hat-intensity I_{top} is calculated to be

$$I_{\text{top}} = \frac{I_{\text{total}}}{B} = \frac{I_0}{B}\sqrt{\frac{\pi}{k}}erf\left(\sqrt{k}\,\frac{D}{2}\right). \tag{4}$$

The local focal length $f(d)$ for a ray hitting the entrance aperture in a distance d from the optical axis, is calculated from the intensity distribution of the incoming beam $I(d)$. The ray has to be redirected to a point in the distance a from the optical axis, so the integrated intensities under the Gaussian I_{total} and under the top-hat function I_{top} are equal for all d:

$$\int_0^d I(x)dx = \frac{I_0}{2}\sqrt{\frac{\pi}{k}}erf\left(\sqrt{k}d\right) = a \cdot I_{\text{top}}. \tag{5}$$

The distance a is calculated by including (4) in (5):

$$a(d) = \frac{B}{2}\frac{erf\left(\sqrt{k}d\right)}{erf\left(\sqrt{k}\,\frac{D}{2}\right)}. \tag{6}$$

Let us assume a distance L of the imaging plane from the optics and the incoming rays to be parallel to the optical axis and the length of the optics itself is negligible compared to its distance to the sample plane. Considering the theorem of intersecting lines the local focal length $f(d)$ is given by

$$f(d) = \frac{Ld}{a(d) - d}. \tag{7}$$

In Fig. 2 the resulting local focal length f is plotted over the distance d of the incoming ray from the optical axis.

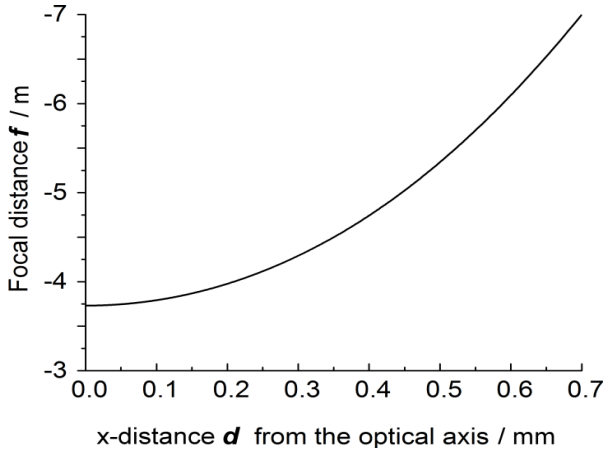

Fig. 2. Example of the local focal length f across the lens' aperture (D = 0.8 mm, L = 30 m)

Based on these findings, the shape of the required refracting surface of the optics is calculated. For compound refractive lenses (CRLs) with biconcave parabolic lens surfaces the lens geometry can be described by

$$R = f2\delta N \tag{8}$$

with the minimum radius R of curvature of the parabola, the photon energy dependent decrement of the refractive index δ of the lens material and the focal length f [13]. Eq. (8) is a good approximation for a focal lengths which is large compared to the physical

Optics EXPRESS

length of the lens [14]. For the requested beam shaper this approximation is applicable, as the distances between the optics and the source as well as the detector plane are in the tens of meter range, whereas the final optics has a total length in the range of a few centimeters only. The parabolic shape of a CRL is described as

$$z = \frac{1}{2R} x^2. \tag{9}$$

In the case of a beam shaper the radius of curvature R varies in x-direction and the resulting refractive surface will not be a parabola. The shape of the resulting refracting surface cannot be described in a closed analytic form. So the shape of the refracting surface has been calculated numerically starting at the optical axis, where the surface is perpendicular to the optical axis. Figure 3(a) shows an example of a single element of a beam shaping optics.

The resulting refracting elements have a lot of absorbing material, especially near the optical axis. Therefore, these elements are converted into a kind of Fresnel-lens [18]. The number N of lens elements is chosen in such a way, that the resulting corner angle β (see Fig. 3(b)) stays larger than 20° for all elements to keep the lens elements technically feasible.

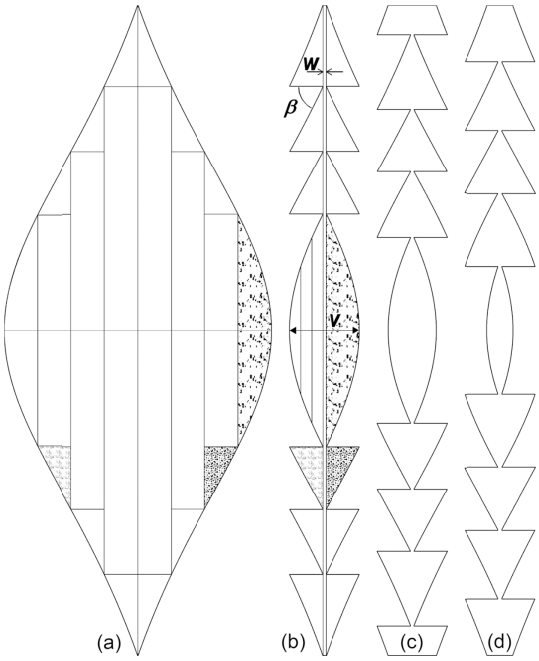

Fig. 3. The underlying principle shape of a single element of these beam shaping optics divided in eight slices is shown in (a). The conversion of (a) into a Fresnel-element is indicated in (b), with a constant thickness w in the center of the optics and the inner corner angle β. The structures in (c) and (d) are Fresnel-elements with modified diameter of the innermost zone forming a block structure together with (a). The group of elements (b), (c), (d) forms the smallest building block for the macroscopic lens to homogenize the projected thickness.

The resulting single lens element is divided into M slices (M = 8 in Fig. 3(a)). Similar to Fresnel-lenses, rectangular blocks of absorbing material are removed. Shifting the remaining parts of the lens towards the center of each lens leads to M-1 Fresnel lens segments. The maximum width of these structures is chosen to end up with technically feasible structure sizes. When simulating the resulting optics made out of a stack of equal Fresnel-lens elements (Fig. 3(b)) the intensity in the detector plane is rather inhomogeneous with variations in the 10-15% range. This is caused by the strong variation of the material thickness and thus absorption of the Fresnel elements. Further improvement of the intensity homogeneity could be achieved by reducing the thickness of the slices, re-

Optics EXPRESS

sulting in smaller Fresnel-structures. This solution is currently not possible due to manufacturing constraints.

This limitation however can be overcome by forming K blocks (the three slices in Fig. 4(b)-4(d) form such a block) of a number of $P = N/K$ different lens elements sliced in different ways instead of using N equal Fresnel-lens elements. In Fig. 3 the Fresnel-elements (b) to (d) form such a block. The P different slices in such a block differ by the thickness of their innermost zone. The thickness v of the innermost zone of the original Fresnel-element is divided by the number P of different slices in one block. The thickness of the innermost structures of the P different lens elements is $m \cdot v/P$ with $m \in \mathbb{N} \cap m \leq P$. As a consequence, the position of the points where the Fresnel-elements are very thin varies within each block. This leads to a much more homogeneous intensity distribution in the detector plane.

3. Lens layout parameters and fabrication

The optics are produced via deep X-ray lithography [19,20] at the KIT synchrotron source. The lens material was chosen to be SU-8 [21], an epoxy based negative resist (type mr-X-50 from mrt, Berlin), processed on a silicon wafer of 525 µm thickness. This lens material has proven to possess a long-term radiation stability at different synchrotron radiation applications up to a deposited dose of 2 MJ/cm^3 [22] and likely above.

The first layout (see Fig. 4) of this type of beam shaping optics was designed and realized for the P05 imaging beamline operated by HZG at the storage ring at PETRA III (DESY, Hamburg Germany) [23,24]. The instrument is optimized for *in situ* experiments in particular to allow for extended sample environments. The field of view (FoV) however is limited due to the nature of the undulator source: The beam height in vertical direction lies in the range of 1.6 mm to 2 mm FWHM at the sample position while the horizontal beam size is around 7 mm. This is an inherent property of undulator sources and not ideal for full field imaging like radiography and tomography since for many sample systems a larger FoV would be beneficial [23]. Until now computed tomography (CT) images of large samples are scanned with several height steps and the tomograms are stacked afterwards. This is very time consuming when it comes to scan time and data processing time and often leads to artefacts in the reconstructed, stitched volume. In particular for *in situ* experiments stacking is of course not an option.

To overcome this limitation and allow for scanning larger sample volumes by *in situ* experiments a novel type of beam enlarging optics was developed. The optics was designed to operate at a photon energy of 24 keV, a source distance of 60 m, and a working distance of 30 m. As the FWHM of the incoming beam was 1.6 mm, a physical entrance aperture of 1.4 mm was chosen. The resulting layout (see Fig. 4) had $N = 20$ elements in blocks of $P = 5$ different slices, each with M-1 = 15 segments. The air gap between neighbor elements was chosen to be 150 µm, the minimum thickness of the elements was $w = 6$ µm, the minimum technically achievable edge rounding radius was 0.5 µm.

Optics EXPRESS

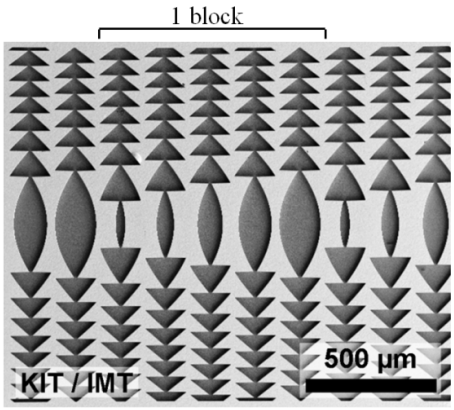

Fig. 4. SEM image of a part of an intermediate X ray absorber mask for beam shaper optics fabrication.

A proof-of-concept experiment was performed with lens structures of 0.8 mm height. The structures' height was limited to 800 µm by the LIGA fabrication process. For this experiment, two structures were aligned face to face to reach 1.6 mm working width. To cover the full beam width, the structures presented here are going to be stacked and pre-aligned in the laboratory to cover the full beam width.

4. Experimental results

A first optical characterization of the optics at the imaging beamline P05 at the storage ring PETRA III, aimed to measure the beam enlargement, the intensity distribution at the detector position as well as the suitability for computed tomography.

Figure 5 shows a projection image of the beam with the beam shaping optics installed in the center. The original beam profile (white areas in Fig. 5(a)) is widened to a vertical size of 5.6 mm (grey area in the center part of Fig. 5(a)) by the beam shaping optics as revealed by the intensity profiles (Fig. 5(b)). For these first tests the optics was placed at a distance of 20 m with respect to the sample. Therefore, the expected widening up to 7 mm could not be realized. The sample to detector distance was 15 mm. In this setup the beam hitting the sample can be assumed to be nearly parallel due to the large optics to sample distance of 20 m. So standard filtered back projection was used for tomographic reconstruction. The horizontal width of the enlarged beam area is 1.6 mm, which results from two beam shaping elements stacked together. Left and right to the enlarged beam one can still recognize the original Gaussian beam with 1.35 mm FWHM. The black stripes in between are due to the two absorbing substrates. In Fig. 5(b) the intensity profile of the enlarged beam (red) is shown in comparison to the nearly Gaussian beam profile (blue). Although the intensity profile is still not perfectly flat, the enlargement of the beam can be seen clearly. The standard deviation of the intensity of the shaped beam profile was about 17 percent of the average intensity. The slight asymmetry of the shaped beam most probably results from the not perfectly Gaussian-shaped incoming beam. The calculated efficiency of the optics was 83%, being the ratio of the integrated intensity of the enlarged beam profile with respect to the integrated intensity of the original Gaussian beam profile. The measured efficiency is 63%. The difference might result from a non-perfect alignment of the micro prisms with respect to the incoming beam.

Optics EXPRESS

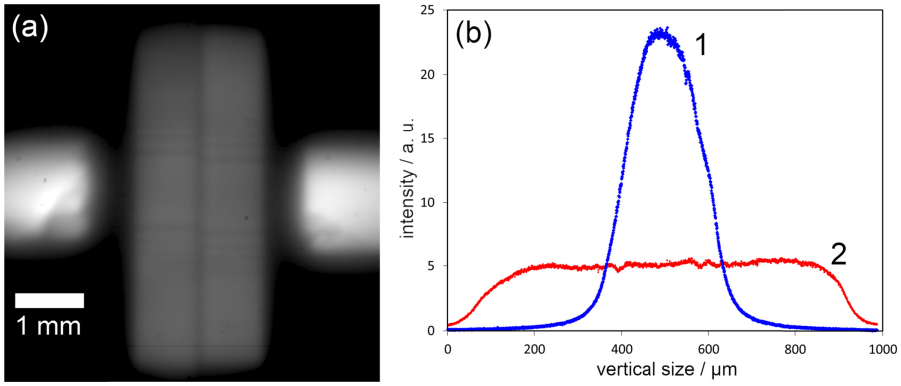

Fig. 5. Result of the beam shaper profile measurement at PETRA III, P05 with 5x magnification and 2.48 µm virtual pixel size in the scintillator plane. (a): In the center the enlarged beam with a FoV of 5.6 mm in vertical direction and 1.6 mm in horizontal direction (two stacked 800 µm beam shaper optics) and on the left and right side of the enlarged beam the original Gaussian beam with 1.6 mm FWHM. (b): Beam profile changes from original Gaussian like (1, blue) to top-hat like intensity distribution (2, red).

To verify the performance of the optics, a 3 mm long tip of a sea urchin spine was chosen as a long and thin test sample. A CT measurement was performed at a photon energy of 24 keV using a $CdWO_4$ scintillation screen and a 10x visible light optical magnification resulting in an effective pixel size of 1.25 µm and a resolution of 3.9 µm line and space. The experimental setup is sketched in Fig. 6. In the detector image in Fig. 6 the sample is visible.

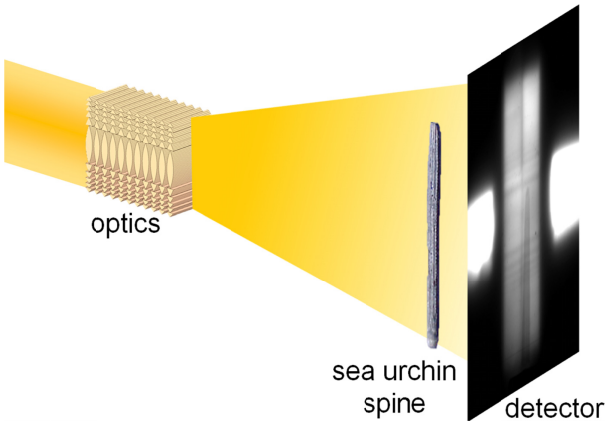

Fig. 6. Principle of the CT measurement setup to investigate a sea urchin spine using the requested beam shaping optics to widen the beam from 1.35 mm to 5.6 mm FWHM in vertical direction. Distances were: source to optics 65 m, detector to optics 21 m.

The mechanical stability and performance of the beam-enlarging optics setup was tested by acquiring a tomography scan. Using the standard CT acquisition scheme of the P05 micro tomography, we could not detect any negative influence on the image quality. The flat-field correction works well and no effects on the homogeneity of the background could be determined (see Fig. 7(a)). The reconstructed volume is not blurred by major artefacts, which could have been introduced by the optics. The image resolution is comparable to the resolution achieved in an image with smaller field of view acquired without the optics. This was also verified by the flat background in the reconstructed slices, where the histogram shows only two distinct peaks: One for air and one for the sample. Reconstructed slices of the sea urchin spine are exemplarily shown in Fig. 7(b) to 7(d), clearly visualizing the porous matrix network in the center column of the spine.

Optics EXPRESS

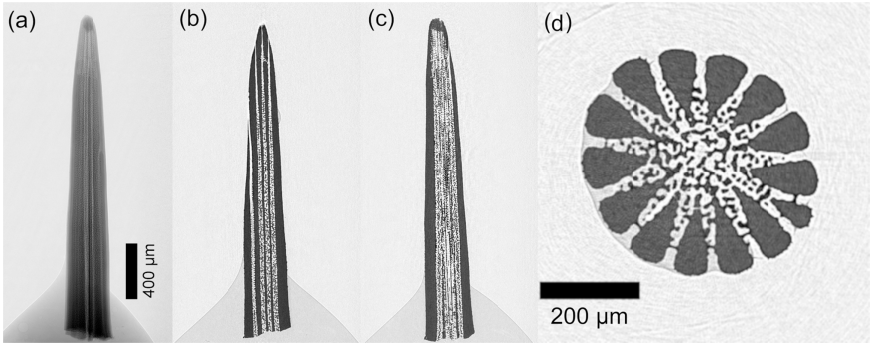

Fig. 7. Tomography of a sea urchin spine using the beam shaper setup: absorption image (a) and reconstructed tomographic slice (b) to (d).

5. Conclusion

The new X-ray optics presented here is designed to overcome beam size limitation at high brilliance 3rd generation synchrotron sources using specially designed refractive X-ray lens elements. The beam shaping optics was fabricated via deep X-ray lithography in an epoxy based photo resist. The optics widens the incoming beam by a factor of four, increasing the field of view in shadow projection imaging. At the same time the intensity profile of the incoming beam is converted from Gaussian like to top-hat like profile. This profile with a more uniform illumination increases the statistics and therefore the image quality in most parts of the field of view. The intensity inhomogeneity was in the range of 17% of the average intensity. In order to cover the whole beam width (horizontal direction), an increase in the structural height is needed. In future it is therefore planned to realize optics with 3 mm resist height. Combining two of these optics and taking into account the beam enlargement due to the beam divergence, an increased field of view of up to 7 mm x 7 mm at the position of the sample will be achievable. Ray tracing simulations have been performed at KIT-IMT on beam shaping optics in different setups. The results showed, that beam shaping optics of this type should be customized for each individual set-up, considering source size and distance, photon energy and distance to the experiment for ideal performance. However, they are of great advantage as they can improve the diversity of methods at synchrotron beamlines, for example for in situ experiments where acquiring multiple height steps is not an option. Fourth generation synchrotron sources (diffraction limited storage rings) like MAX IV (Lund) will decrease the beam size even further. One option for full field micro tomography beamlines is to build the experiment far from the source (undulator) in order to achieve a decent sized field of view. Another option is to defocus the beam by e. g. using mirrors, the costs of such optics however are also not negligible and the time needed for alignment is also significant. Beam shaping optics, like the ones presented here, are therefore an attractive alternative.

Funding

Helmholtz Association (VH-VI-428, Virtual Institute New X-ray analytic Methods in Material science); Helmholtz Association (Karlsruhe Nano Micro Facility, KNMF); Karlsruhe School of Optics & Photonics (KSOP); German Research Foundation (DFG) (SFB 986 “M3”, project Z2).

References

1. P. C. Johns and M. J. Yaffe, “X-ray characterisation of normal and neoplastic breast tissues,” Phys. Med. Biol. **32**(6), 675–695 (1987).
2. I. Manke, Ch. Hartnig, M. Grünerbel, W. Lehnert, N. Kardjilov, A. Haibel, A. Hilger, J. Banhart, and H. Riesemeier, “Investigation of water evolution and transport in fuel cells with high resolution synchrotron x-ray radiography,” Appl. Phys. Lett. **90**(17), 174105 (2007).
3. L. Salvo, P. Cloetens, E. Maire, S. Zabler, J. J. Blandin, J. Y. Buffière, W. Ludwig, E. Boller, D. Bellet, and C. Josserond, “X-ray micro-tomography an attractive characterisation technique in materials science,” Nucl. Inst. & Meth. Sect. B **200**, 273–286 (2003).

Optics EXPRESS

4. J. Baruchel, J. Y. Buffiere, and E. Maire, *X-ray tomography in material science* (Hermes science publications, 2000), ISBN 2 7462–0115–1.
5. F. Marschall, A. Last, M. Simon, M. Kluge, V. Nazmov, H. Vogt, M. Ogurreck, I. Greving, and J. Mohr, "X-ray full field microscopy at 30 keV," J. Phys. Conf. Ser. **499**, 012007 (2014).
6. U. Bonse, F. Busch, O. Günnewig, F. Beckmann, R. Pahl, G. Delling, M. Hahn, and W. Graeff, "3D computed X-ray tomography of human cancellous bone at 8 μm spatial and 10–4 energy resolution," Bone Miner. **25**(1), 25–38 (1994).
7. A. Blanke, B. Wipfler, H. Letsch, M. Koch, F. Beckmann, R. Beutel, and B. Misof, "Revival of Palaeoptera-head characters support a monophyletic origin of Odonata and Ephemeroptera (Insecta)," Cladistics **28**(6), 560–581 (2012).
8. K.-J. Kim, "Brightness, coherence and propagation characteristics of synchrotron radiation," Nucl. Instrum. Methods Phys. Res. A **246**(1-3), 71–76 (1986).
9. N. A. Vinokurov, O. A. Shevchenko, and V. G. Tcheskidov, "Variable-period permanent magnet undulators," Phys. Rev. Spec. Top. Accel. Beams **14**(4), 040701 (2011).
10. J. Hsieh, *Computed tomography: Principles, design, artefacts, and recent advances* (SPIE and John Wiley & Sons Inc., 2009), 2nd edition, ISBN 9780819475336.
11. M. Engelhardt, J. Baumann, M. Schuster, C. Kottler, F. Pfeiffer, O. Bunk, and C. David, "High-resolution differential phase contrast imaging using a magnifying projection geometry with a microfocus X-ray source," Appl. Phys. Lett. **90**(22), 224101 (2007).
12. F. M. Dickey, *Laser beam shaping: Theory and techniques* (CRC, 2014, pp. 367–403), 2nd edition, ISBN: 978–1-4665–6100–7.
13. A. Snigirev, V. Kohn, I. Snigireva, and B. Lengeler, "A compound refractive lens for focusing high energy X-rays," Nature **384**(6604), 49–51 (1996).
14. B. Lengeler, C. G. Schroer, B. Benner, A. Gerhardus, T. F. Günzler, M. Kuhlmann, J. Meyer, and C. Zimprich, "Parabolic refractive X-ray lenses," J. Synchrotron Radiat. **9**(3), 119–124 (2002).
15. C. G. Schroer, M. Kuhlmann, U. T. Hunger, T. F. Günzler, O. Kurapova, S. Feste, F. Frehse, B. Lengeler, M. Drakopoulos, A. Somogyi, A. S. Simionovici, A. Snigirev, I. Snigireva, C. Schug, and W. H. Schröder, "Nanofocusing parabolic refractive x-ray lenses," Appl. Phys. Lett. **82**(9), 1485–1487 (2003).
16. F. Marschall, A. Last, M. Simon, H. Vogt, and J. Mohr, "Simulation of aperture-optimised refractive lenses for hard X-ray full field microscopy," Opt. Express **24**(10), 10880–10889 (2016).
17. E. Kornemann, O. Márkus, A. Opolka, T. Zhou, I. Greving, M. Storm, C. Krywka, A. Last, and J. Mohr, "Miniaturized compound refractive X-ray zoom lens," Opt. Express **25**(19), 22455–22466 (2017).
18. M. A. Fresnel, "Mémoire sur un nouveau système d'éclairage des phares," l'imprimerie royale, Paris, (1822).
19. V. Nazmov, L. Shabel'nikov, F.-J. Pantenburg, J. Mohr, E. Reznikova, A. Snigirev, I. Snigireva, S. Kouznetsov, and M. DiMichiel, "Kinoform X-ray lens creation in polymer materials by deep X-ray lithography," Nucl. Instrum. Methods Phys. Res. **217**(3), 409–416 (2004).
20. V. Nazmov, E. Reznikova, J. Mohr, A. Snigirev, I. Snigireva, S. Achenbach, and V. Saile, "Fabrication and preliminary testing of X-ray lenses in thick SU-8 resist layers," Microsyst. Technol. **10**(10), 716–721 (2004).
21. A. L. Bogdanov and S. Peredkov, "Use of SU-8 photoresist for very high aspect ratio X-ray lithography," Microelectron. Eng. **53**(1-4), 493–496 (2000).
22. C. Krywka, A. Last, F. Marschall, O. Márkus, S. Georgi, M. Müller, and J. Mohr, "Chr. Krywka, A. Last, F. Marschall, O. Márkus, S. Georgi, M. Müller and J. Mohr, "Polymer compound refractive lenses for hard X-ray nanofocusing," AIP Conf. Proc. **1764**, 020001 (2016).
23. I. Greving, F. Wilde, M. Ogurreck, J. Herzen, J. U. Hammel, A. Hipp, F. Friedrich, L. Lottermoser, T. Dose, H. Burmester, M. Müller, and F. Beckmann, "P05 imaging beamline at PETRA III: first results," Proc. SPIE **9212**, 92120O (2014).
24. F. Wilde, M. Ogurreck, I. Greving, J. U. Hammel, F. Beckmann, A. Hipp, L. Lottermoser, I. Khokhriakov, P. Lytaev, Th. Dose, H. Burmester, M. Müller, and A. Schreyer, "Micro-CT at the imaging beamline P05 at PETRA III," AIP Conf. Proc. **1741**, 030035 (2016).